Scientific Reports

https://doi.org/10.1038/s41598-026-65280-3

Article in Press

Reliability-constrained cost optimization of standalone photovoltaic water pumping systems under time-structured irrigation demand

Received: 31 May 2026

Accepted: 30 July 2026

Published online: 08 August 2026

Cite this article as: Demirci A., Özgür P., Terkes M. *et al.* Reliability-constrained cost optimization of standalone photovoltaic water pumping systems under time-structured irrigation demand. *Sci Rep* (2026). https://doi.org/10.1038/s41598-026-65280-3

Alpaslan Demirci, Pelin Özgür, Musa Terkes, Idriss Dagal & Umit Cali

We are providing an unedited version of this manuscript to give early access to its findings. Before final publication, the manuscript will undergo further editing. Please note there may be errors present which affect the content, and all legal disclaimers apply.

If this paper is publishing under a Transparent Peer Review model then Peer Review reports will publish with the final article.

ARTICLE IN PRESS

© The Author(s) 2026. **Open Access** This article is licensed under a Creative Commons Attribution 4.0 International License, which permits use, sharing, adaptation, distribution and reproduction in any medium or format, as long as you give appropriate credit to the original author(s) and the source, provide a link to the Creative Commons licence, and indicate if changes were made. The images or other third party material in this article are included in the article's Creative Commons licence, unless indicated otherwise in a credit line to the material. If material is not included in the article's Creative Commons licence and your intended use is not permitted by statutory regulation or exceeds the permitted use, you will need to obtain permission directly from the copyright holder. To view a copy of this licence, visit http://creativecommons.org/licenses/by/4.0/.

ARTICLE IN PRESS

Reliability-Constrained Cost Optimization of Standalone Photovoltaic Water Pumping Systems under Time-Structured Irrigation Demand

Alpaslan Demirci[a], Pelin Özgür[a], Musa Terkes[a], Idriss Dagal[b], Umit Cali[c,d,e,*]

[a]*Department of Electrical Engineering, Yildiz Technical University, 34220 Istanbul, Türkiye*
[b]*Department of Electrical-Electronics Engineering, Istanbul Beykent University, 34396 Istanbul, Türkiye*
[c]*Department of Electric Power Engineering, Norwegian University of Science and Technology, 7034 Trondheim, Norway*
[d]*School of Physics, Engineering and Technology, University of York, YO10 5DD York, United Kingdom*
[e]*Artificial Intelligence, Smart Infrastructure and Robotics Research Center, American University of Sharjah, Sharjah, United Arab Emirates*

Abstract

Photovoltaic (PV)-powered water pumping systems (WPS) are increasingly used for agricultural irrigation, yet their reliability is governed not only by annual energy balance but also by the timing of water withdrawal relative to solar availability and hydraulic storage recovery. This study develops a reliability-constrained simulation–optimization framework for a standalone PV water pumping system (PVWPS) in Konya, Türkiye, and evaluates four equal-daily-volume irrigation demand topologies: uniform, morning-only, split morning–evening, and greenhouse-pulsed demand. To address the stochastic and mixed-integer nature of the sizing problem, the analysis validates the metaheuristic search using an enumeration-refined design-space check, distinguishes nominal boundary designs from uncertainty-aware margin designs, and adds sensitivity analyses for seasonal demand redistribution, groundwater-head increase, evaporation, pump-efficiency degradation, transient power loss, and pulse-window flow adequacy. Enumeration-refined nominal designs satisfy the deterministic reliability target, with optimal PV capacities between 2.52 and 2.70 kW and hydraulic storage volumes between 27.10 and 29.80 m^3. Relative to uniform demand, the morning-only, split, and greenhouse-pulsed profiles reduce equivalent shortage duration by approximately 72%, 54%, and 58%, respectively, while cost-of-water differences remain moderate. Monte Carlo testing shows that deterministic just-feasible designs are sensitive to demand uncertainty; tightening the nominal LLP target from 0.010 to 0.008 reduces the mean Monte Carlo LLP below 0.010 for all scenarios, but does not guarantee strict high-percentile chance-constrained feasibility. The results indicate that irrigation timing is an important operational co-design factor for hydraulic storage and shortage exposure, while practical deployment requires explicit robustness margins when groundwater drawdown, uncovered storage evaporation, pump degradation, or sub-hourly transients are expected.

Keywords: Photovoltaic water pumping, irrigation demand timing, reliability-constrained sizing, water storage tank, loss of load probability, techno-economic optimization, demand uncertainty, PV curtailment, robustness margin

*Corresponding author.
Email address: umit.cali@ntnu.no (Umit Cali)

ARTICLE IN PRESS

Nomenclature

Symbol	Unit	Description
A_{tank}	m^2	Effective exposed water-surface area of the storage tank
a_{SAPM}	–	Empirical SAPM module-temperature coefficient associated with the mounting configuration
b_{SAPM}	s/m	Empirical SAPM wind-speed coefficient associated with the mounting configuration
C_{inv}	\$	Initial investment cost
$C_{\text{O\&M},y}$	\$/year	Operation and maintenance cost in year y
$C_{\text{rep},y}$	\$	Replacement cost in year y
D_t	L/h	Irrigation water demand at hour t
D_{base}	L/h	Baseline hourly irrigation demand
D_t^{MC}	L/h	Perturbed hourly irrigation demand in a Monte Carlo realization
D_t^{served}	L/h	Served irrigation demand at hour t
D_t^{unmet}	L/h	Unmet irrigation demand at hour t
$D_{\text{sd}}^{\text{eq}}$	days/year	Equivalent shortage duration, computed as annual shortage hours divided by 24
$D_{\text{sd,max}}^{\text{eq}}$	days/year	Maximum allowable equivalent shortage duration
E_t^{evap}	L/h	Evaporative water loss from the storage tank at hour t
f_{der}	–	Overall PV derating factor
g	m/s^2	Gravitational acceleration
$G_{\text{POA}}(t)$	W/m^2	Plane-of-array irradiance at hour t
G_{ref}	W/m^2	Reference irradiance under standard test conditions
H_{lift}	m	Vertical lifting head
$H_{\text{loss}}(Q_t)$	m	Hydraulic head loss as a function of pump flow rate
H_{sd}	h/year	Annual number of hourly time steps with unmet demand
H_{static}	m	Static pumping head
$H_{\text{TDH}}(t)$	m	Total dynamic head at hour t
$h(t)$	–	Hour-of-day index corresponding to hourly time step t
$\mathbb{I}(\cdot)$	–	Indicator function
$J(\mathbf{x})$	$\text{\$/m}^3$	Penalty-augmented objective function
K_t	–	Daily clearness index
N	years	Project lifetime
N_{pop}	–	Population size of the GWO algorithm
P	–	Number of parallel PV strings
P_{min}, P_{max}	–	Lower and upper bounds of the number of parallel PV strings
$P_{\text{avail}}(t)$	W	Available electrical power delivered to the pump drive
$P_{\text{dc}}(t)$	W	PV DC output power at hour t
$P_{\text{dc,STC}}$	W	Installed PV DC capacity under standard test conditions
$P_{\text{hyd}}(t)$	W	Hydraulic power at hour t
$P_{\text{mpp,STC}}$	W	PV module maximum power at standard test conditions
P_t^{PV}	W	PV-generated power at hour t
P_t^{unused}	W	Unused or curtailed PV power at hour t
Q_t	L/h	Realizable pump flow rate at hour t
Q_t^{in}	L/h	Pumped inflow to the storage tank at hour t
Q_{max}	L/h	Maximum feasible pump flow rate
r	–	Real discount rate
S	–	Number of PV modules connected in series
S_{min}, S_{max}	–	Lower and upper bounds of the number of series-connected PV modules
t	–	Hourly simulation index
$T_{\text{air}}(t)$	°C	Ambient temperature at hour t
$T_c(t)$	°C	PV cell temperature at hour t
$T_m(t)$	°C	PV module back-surface temperature at hour t
T_{max}	–	Maximum number of GWO iterations

ARTICLE IN PRESS

ARTICLE IN PRESS

Symbol	Unit	Description
T_{ref}	°C	Reference temperature under standard test conditions
ΔT_{SAPM}	°C	SAPM cell-to-module temperature difference at reference irradiance
V_t	L	Water volume in the storage tank at hour t
$V_{\mathrm{delivered}}(\mathbf{x})$	L/year	Total annual delivered water volume for design $\mathbf{x}$
$V_{\max}$	L	Tank storage capacity and continuous storage decision variable
$V_{\max}^{\mathrm{up}}$	L	Upper bound of the admissible tank-capacity range
$V_{\min}$	L	Lower bound of the admissible tank-capacity range
$V_{\mathrm{tank}}^{\mathrm{crit}}$	L	Critical tank capacity satisfying the LLP constraint
$v_w(t)$	m/s	Wind speed at hour t
$\mathbf{x}$	–	Design vector, $\mathbf{x} = [S, P, V_{\max}]$
y	–	Economic evaluation-year index
α	\$/m^3	Penalty coefficient for LLP-constraint violation
$\alpha_h^{(s)}$	–	Normalized hourly demand multiplier for scenario s
β	\$ m^{-3} (day/year)$^{-1}$	Penalty coefficient for equivalent-shortage-duration violation
ϵ_t	–	Normally distributed hourly demand noise at hour t
η_t	–	Bounded hourly multiplicative demand factor, $\eta_t = \mathrm{clip}(1 + \epsilon_t, 0.2, 2.0)$
η_{el}	–	Overall electrical conversion efficiency
η_p	–	Net pump–motor efficiency
ρ_w	kg/m^3	Water density
σ_h	–	Standard deviation of the hourly demand noise in the Monte Carlo analysis
ξ_t	–	Generic demand modifier in the scenario-demand equation; set to unity for nominal demand profiles
ζ	–	Realization-level demand-scaling factor sampled from $\mathcal{U}(0.85, 1.15)$ in the Monte Carlo analysis
$\mathrm{LLP}_{\max}$	–	Maximum allowable loss of load probability
Abbreviations		
BEP	–	Best efficiency point
CAPEX	–	Capital expenditure
COU	\$/m^3	Cost of water
ESD	days/year	Equivalent shortage duration
GWO	–	Grey Wolf Optimizer
LLP	–	Loss of load probability
LPSP	–	Loss of power supply probability
MPPT	–	Maximum power point tracking
NOCT	°C	Nominal operating cell temperature
NPV	\$	Net present value
O&M	–	Operation and maintenance
POA	–	Plane-of-array
PSO	–	Particle swarm optimization
PV	–	Photovoltaic
PVGIS	–	Photovoltaic Geographical Information System
PVWPS	–	Photovoltaic water pumping system
SAPM	–	Sandia Array Performance Model
STC	–	Standard test conditions
TDH	m	Total dynamic head
TMY	–	Typical meteorological year
WPS	–	Water pumping system

1. Introduction

Solar photovoltaic (PV) water pumping is increasingly adopted as a technically mature alternative to diesel-fuelled pumping for agricultural water supply in off-grid and weak-grid regions, since it couples local renewable generation with a hydraulic storage buffer and re-

ARTICLE IN PRESS

moves recurring fuel logistics and emissions [1]. The relevance of this technology is particularly high in semi-arid agricultural basins, where the water–energy–food nexus is shaped jointly by groundwater dependency, energy price volatility, and irrigation scheduling constraints [2]. Continuous groundwater abstraction in such basins induces a transient cone of depression that raises the static lift over the pumping season, and borehole-level models developed for PV pumping applications show that this drawdown component, together with the nominal static water level, is a first-order driver of life-cycle cost and reliability that is frequently simplified in sizing studies [3]. Field and techno-economic evidence from semi-arid groundwater-irrigation contexts corroborates this sensitivity: total system head and site solar resource jointly govern the economics of PV groundwater pumping in West Africa [4], experimental campaigns in the Algerian Sahara report head- and temperature-driven performance degradation relative to nameplate design [5], and techno-economic assessments in arid and desert climates show that pumping-head assumptions materially shift the optimal tilt and sizing strategy [6]. Photovoltaic water pumping systems (PVWPSs) should therefore not be interpreted only as energy-conversion assets; they are coupled water–energy systems in which solar-resource variability, pumping head, reservoir dynamics, and irrigation timing jointly determine water-service reliability. In the Konya case considered here, high groundwater dependency makes this coupling especially consequential, because aquifer drawdown and recovery conditions can alter both the energy requirement and the reliability margin of a nominally feasible design.

A substantial body of work has addressed PVWPS component modeling and techno-economic sizing. Early reviews established the baseline architecture of PV-array, motor-pump, and storage subsystems and catalogued the reliability and cost trade-offs against diesel alternatives [7], while subsequent studies proposed dedicated sizing procedures that jointly select PV array and reservoir capacity under a target reliability constraint [8]. Multi-criteria and multi-stage formulations extended this baseline sizing problem to account for user comfort and simultaneous PV-tank sensitivity [9, 10], and hybridization with wind or diesel back-up has been examined for semi-arid irrigation sites where solar resource alone cannot guarantee year-round supply [11]. Reliability quantification has evolved from electrical indices such as loss of power supply probability (LPSP) toward water-service indicators; case studies report water-shortage-probability and LPSP jointly for small-scale citrus irrigation [12], while comparative assessments across climate zones [13] and dedicated reliability evaluations of underground PV pumping [14] show that the choice of reliability index and simulation resolution both influence the reported design margin. Economic performance is typically expressed through life-cycle cost, net present value, or a levelized cost of water (COU), and comprehensive techno-economic studies combining these metrics with feasibility screening remain common in the literature [15]. Storage-side variations have also been explored, including tank-battery-grid hybrids in Egypt [16], urban pressurized networks supplied by direct PV pumping with either tank or battery buffering [17], agrivoltaic rainwater-harvesting reservoirs [18], wastewater-treatment facilities coupled to pumped storage and small hydro for autonomous operation [19], and multi-energy complementary configurations for hose-drawn traveler irrigation equipment in China [20]. Complementary experimental and field-validation studies from Spain [21], Algeria [22], and Nepal [23] further indicate that reported performance and cost figures are strongly site- and configuration-specific, reinforcing the need for transparent, reproducible sizing frameworks rather than generalized rules of thumb.

Optimization methodology is a second major strand of this literature. Because PVWPS sizing couples discrete array configurations with continuous storage capacity under a non-convex reliability constraint, metaheuristic search has become the default solution approach;

ARTICLE IN PRESS

the grey wolf optimizer (GWO) itself [24] and its improved variants [25] are among the most widely applied, alongside artificial-rabbits [26], chaotic horse-herd [27], and other nature-inspired algorithms benchmarked broadly across engineering problems [28, 29]. Reviews of hybrid and metaheuristic sizing methods for renewable-energy systems emphasize that algorithm choice alone rarely guarantees global optimality on mixed discrete–continuous landscapes and recommend multi-run or benchmark-based validation [30, 31, 32, 33]. In parallel, a distinct body of PVWPS work focuses on converter- and motor-level control rather than system sizing, including maximum-power-point tracking (MPPT) under partial shading [34, 35], sliding-mode and field-oriented control of induction-motor drives [36, 37], fuzzy-logic and Kalman-filter-assisted tracking [38, 39], and nutcracker- or gorilla-troop-inspired optimizers applied to combined MPPT and flow-rate objectives [40, 41, 42]; these studies establish that power-electronic and control-loop losses are non-trivial but are typically treated as a separate optimization layer from array-tank capacity sizing, which is the layer addressed here. PV-array electrical behavior itself is commonly represented through datasheet-based single-diode parameter extraction [43] and standard MPPT reviews [44], while site solar-resource characterization increasingly relies on open, standardized irradiance data access tools [45], an approach also adopted in the present study. Despite this breadth, multi-run convergence statistics, benchmarking against a second metaheuristic, and exhaustive-search validation remain the exception rather than the rule in the PVWPS sizing literature, a gap that motivates the optimizer-validation strategy adopted in Section 2.

The methodological gap addressed here is more specific than algorithm choice. Most PVWPS sizing studies aggregate irrigation demand into a single daily or seasonal profile, which makes it difficult to isolate how the intra-day timing of an otherwise identical daily water volume changes storage recovery, shortage persistence, and PV curtailment. A recent study synergizing irrigation patterns with PV pumping sizing across diverse agro-climatic zones in India represents the closest prior treatment of demand timing as a design input [46], but it evaluates timing jointly with static head across zones rather than isolating the timing effect under a controlled, equal-daily-volume comparison, and it does not report an hour-resolved, tank-state-aware shortage diagnostic. The present study differs by holding daily water volume fixed across four intra-day demand topologies – continuous, morning-dominant, split morning–evening, and greenhouse-style pulsed irrigation – so that differences in COU, reliability, storage sizing, and shortage timing can be attributed to demand topology rather than to demand magnitude. This equal-volume construction is intentionally a diagnostic device: it isolates the timing effect but does not imply that real precision-irrigation systems draw an invariant daily volume, so seasonal and crop-specific evapotranspiration effects are examined separately through dedicated sensitivity analysis and discussed as a limitation rather than folded into the main design comparison.

A second gap concerns robustness under demand uncertainty. Deterministic nominal designs that satisfy a loss-of-load-probability (LLP) target under one fixed demand realization can fail to satisfy the same target once daily demand magnitude or intra-day distribution is perturbed. Within the PVWPS sizing studies reviewed above, deterministic point estimates predominate, motivating an explicit uncertainty stress test; related hybrid-system research also illustrates the value of reporting solution dispersion rather than a single deterministic outcome [33]. The present analysis does not attempt to solve the full chance-constrained sizing problem; instead, it distinguishes nominal deterministic feasibility from mean-robust feasibility under Monte Carlo demand perturbation and from stricter high-percentile chance-constrained feasibility, reports nominal boundary designs together with their uncertainty sensitivity, and introduces a robustness-margin design that quantifies the additional cost and capacity required to tighten the nominal reliability target.

ARTICLE IN PRESS

The study addresses these gaps through four methodological elements. First, the novelty statement is positioned around demand-topology-controlled comparison and tank-state-aware diagnostics rather than around established component models in isolation. Second, the optimization result is checked against an enumeration-refined search over the admissible mixed-integer PV-configuration and tank-capacity grid, together with a computationally-constrained multi-seed re-check of the metaheuristic search itself. Third, deterministic designs are explicitly evaluated under demand uncertainty and compared with robustness-margin alternatives. Fourth, physical-scope sensitivity analyses quantify the effects of groundwater-head increase, seasonal demand redistribution, tank evaporation, pump-efficiency degradation, transient PV loss, and pulse-window flow adequacy. The principal contributions are therefore:

- A controlled comparison of four intra-day irrigation demand topologies under equal daily water volume, separating the timing effect on COU, LLP, equivalent shortage duration, storage capacity, and PV curtailment from total demand magnitude.
- A tank-state-aware reliability diagnostic that links annual LLP and shortage-duration outcomes to hour-resolved storage depletion, recovery, and shortage-occurrence signatures.
- An enumeration-refined validation of the mixed-integer sizing results, supplemented by a multi-seed metaheuristic re-check, reducing reliance on a single convergence trace and clarifying the discrete design-space topology.
- A robustness-margin assessment showing how deterministic just-feasible designs behave under stochastic demand perturbation and how a tighter nominal reliability target improves mean performance under uncertainty.
- A physical-scope assessment quantifying how groundwater-head increase, evaporation, pump-efficiency degradation, sub-hourly transient-loss representation, and pulse-window demand affect the reliability interpretation of boundary designs.

ARTICLE IN PRESS

The remainder of the paper is organized as follows. Section 2 presents the case study, physical model, demand scenarios, reliability metrics, optimization procedure, and additional validation analyses. Section 3 reports the numerical results and sensitivity analyses. Section 4 discusses limitations and future research directions. Section 5 concludes the study.

2. Methodology

This study develops an hourly simulation–optimization framework for a standalone PVWPS with hydraulic storage. The system contains no grid backup and no electrochemical battery, so the water tank is the only buffer between intermittent PV generation and irrigation withdrawal. This modeling choice isolates the interaction between PV sizing, hydraulic storage capacity, and demand timing. It also means that the results should be interpreted as representative of a water-storage-dominant PVWPS; battery-assisted smoothing of sub-hourly transients is outside the primary scope and is considered in the limitations.

2.1. Case study and data sources

The case study is located in Konya, Türkiye (37.87°N, 32.49°E), a semi-arid agricultural region with strong solar resource availability and high groundwater dependency. Hourly meteorological data are obtained from the PVGIS database using the SARAH3 product, including

ARTICLE IN PRESS

irradiance, ambient temperature, and wind speed [47]. The retrieved horizontal irradiance components are transposed to plane-of-array (POA) irradiance using a fixed south-facing PV array with tilt angle 16.24° and azimuth 180°. Monthly averages of daily irradiation, ambient temperature, and clearness index are shown in Figure 1. These data define the annual solar-resource boundary condition used in the hourly simulations.

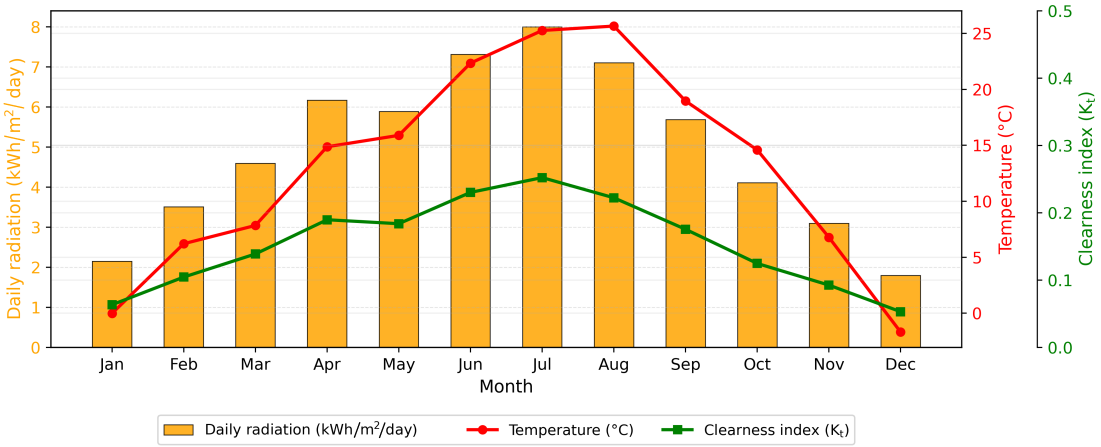


Figure 1: Monthly averages of daily solar irradiation, ambient temperature, and clearness index (K_t) for Konya, Türkiye.

2.2. System configuration and physical modeling

The modeled PVWPS consists of a PV array, MPPT-based power conditioning, a motor–pump unit, hydraulic conveyance line, and a finite water-storage reservoir (Figure 2). The schematic should be interpreted as a physical architecture rather than as a complete set of optimization constraints. Minimum safe-flow and best-efficiency-point constraints are not imposed as separate decision constraints; instead, hydraulic feasibility is represented through the adopted pump-curve and flow-limiting model.

ARTICLE IN PRESS

ARTICLE IN PRESS

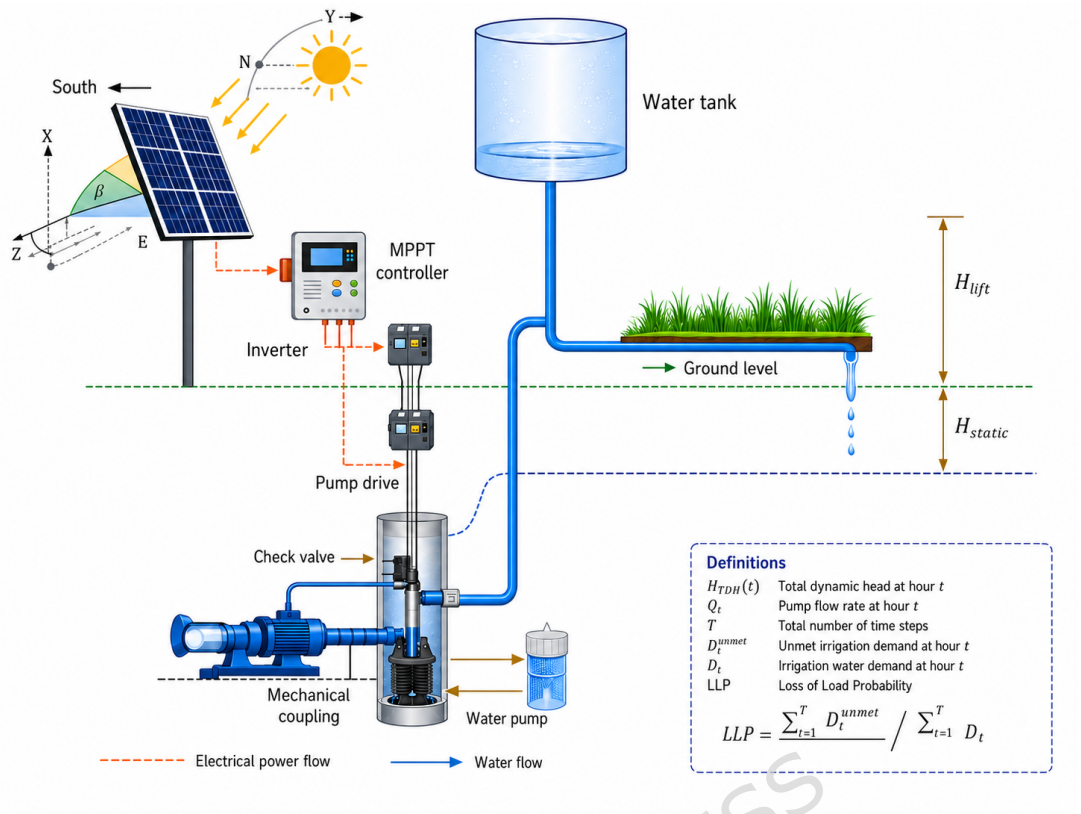


Figure 2: Schematic representation of the standalone PV-powered water pumping system and its principal physical components.

For an array with S modules in series and P strings in parallel, installed DC capacity is

$$P_{\mathrm{dc,STC}} = SPP_{\mathrm{mpp,STC}}. \tag{1}$$

In the numerical implementation, PV output is generated through the `pvlib` model chain using the De Soto DC model and the Sandia Array Performance Model (SAPM) temperature formulation. To ensure reproducibility, the manuscript presents the temperature equations actually used in the computational workflow rather than a nominal operating cell temperature (NOCT) surrogate:

$$T_m(t) = T_{\mathrm{air}}(t) + G_{\mathrm{POA}}(t)\exp(a_{\mathrm{SAPM}} + b_{\mathrm{SAPM}}v_w(t))\,, \tag{2}$$

$$T_c(t) = T_m(t) + \frac{G_{\mathrm{POA}}(t)}{G_{\mathrm{ref}}}\Delta T_{\mathrm{SAPM}}, \tag{3}$$

where T_m is module back-surface temperature, v_w is wind speed, and a_{SAPM}, b_{SAPM}, and ΔT_{SAPM} are mounting-configuration parameters used by the SAPM temperature model. The DC output is then evaluated from the adopted `pvlib` module model and converted to available pump-drive power as

$$P_{\mathrm{avail}}(t) = \eta_{\mathrm{el}}P_{\mathrm{dc}}(t). \tag{4}$$

The Table 1 is included to make clear which model components are implemented directly and to avoid mixing a NOCT analytical surrogate with the SAPM temperature model used in `pvlib`.

ARTICLE IN PRESS

Table 1: PV sub-model settings and numerical inputs used in the hourly simulation.

Parameter / item	Symbol	Setting / value	Source / implementation
PV module	–	Canadian Solar CS5C 90M	`pvlib`/SAM database
Module rated power	$P_{\mathrm{mpp,STC}}$	90 W	Nameplate/database value
Array tilt angle	θ_{tilt}	16.24°	Case-study setting
Array azimuth angle	γ	180°	South-facing array
Albedo	–	0.30	Ground-reflection input
DC model	–	De Soto	`pvlib` model chain
Temperature model	–	SAPM	`pvlib` temperature model
Loss / derating model	f_{der}	PVWatts loss model	Aggregate loss implementation
MPPT/electrical efficiency	η_{el}	0.96	MPPT efficiency setting
Transposition model	–	Isotropic	POA irradiance calculation
Airmass model	–	Kasten–Young 1989	Optical path correction
Clear-sky model	–	Ineichen	Reference irradiance modeling
Racking model	–	Open rack	SAPM mounting assumption
Reference irradiance	G_{ref}	1000 W/m^2	STC reference
Reference temperature	T_{ref}	25°C	STC reference

The total dynamic head is represented as

$$H_{\mathrm{TDH}}(t) = H_{\mathrm{static}} + H_{\mathrm{lift}} + H_{\mathrm{loss}}(Q_t), \tag{5}$$

where the baseline static head is 51 m, the pipe length is 20 m, and the pipe diameter is 0.1016 m. The pump is represented using the manufacturer pump file `SCB_10_150_120_BL.txt` and the Kou-based pump-modeling method implemented in the simulation workflow. The simplified analytical relationship used to describe the water-balance coupling is

$$Q_t = 3.6 \times 10^6 \frac{\eta_p P_{\mathrm{avail}}(t)}{\rho_w g H_{\mathrm{TDH}}(t)}, \tag{6}$$

where Q_t is expressed in L/h and the factor 3.6×10^6 converts the SI result from m^3/s to L/h. Pump-curve feasibility limits are imposed through the numerical model. Because pump efficiency and short-duration transients may vary in practice, additional sensitivity analyses are reported in Section 3.4, rather than assuming that a constant net efficiency fully resolves the pump operating map.

The reservoir is updated at hourly resolution using the saturated mass balance

$$V_{t+1} = \min[V_{\max}, \max(0,\, V_t + (Q_t - D_t)\,\Delta t)]\,, \qquad \Delta t = 1 \text{ h}. \tag{7}$$

The baseline model assumes covered or evaporation-minimized storage. For uncovered storage, the corresponding sensitivity formulation is

$$V_{t+1} = \min[V_{\max}, \max(0,\, V_t + (Q_t - D_t - E_t^{\mathrm{evap}})\,\Delta t)]\,, \qquad \Delta t = 1 \text{ h}, \tag{8}$$

where E_t^{evap} denotes the hourly evaporative water-loss rate. This term is not included in the baseline optimization but is used to quantify the reliability effect of evaporation in the sensitivity analysis.

2.3. Scenario-based irrigation demand modeling

Four demand topologies are considered: uniform demand (S1), morning-only demand (S2), split morning–evening demand (S3), and greenhouse-type pulsed demand (S4). Each scenario is defined through a normalized 24-hour multiplier vector $\boldsymbol{\alpha}^{(s)} = \{\alpha_h^{(s)}\}_{h=0}^{23}$ satisfying

$$\frac{1}{24}\sum_{h=0}^{23} \alpha_h^{(s)} = 1. \tag{9}$$

ARTICLE IN PRESS

The hourly demand is

$$D_t = D_{\text{base}} \alpha_{h(t)}^{(s)} \xi_t, \tag{10}$$

where $D_{\text{base}} = 360$ L/h, corresponding to 6 L/min and 8.64 m^3/day. The unit-mean multiplier assumption is used to isolate intra-day timing while holding total daily water volume constant. It is therefore a controlled diagnostic assumption rather than a crop-specific evapotranspiration model. Seasonal redistribution of the same annual water volume is tested separately in Section 3.3.

S1 represents the continuous-withdrawal assumption often used in preliminary sizing. S2 represents morning-dominant irrigation, relevant where early application is preferred to reduce evaporative losses and avoid peak daytime heat. S3 represents split morning–evening scheduling, which avoids midday application but extends withdrawal into non-solar hours. S4 emulates greenhouse-type pulsed irrigation with relatively intense short-duration withdrawals used to maintain root-zone moisture. These profiles are representative timing structures, not field-measured prescriptions for a specific crop.

2.4. Reliability, economics, and objective function

Unmet water demand is computed as

$$D_t^{\text{unmet}} = \max\left[0,\, D_t - \left(Q_t + \frac{V_t}{\Delta t}\right)\right], \qquad \Delta t = 1 \text{ h}. \tag{11}$$

The volumetric reliability indicator is LLP:

$$\text{LLP} = \frac{\sum_{t=1}^{8760} D_t^{\text{unmet}}}{\sum_{t=1}^{8760} D_t}. \tag{12}$$

The duration-based reliability indicator is equivalent shortage duration (ESD). Shortage hours are first counted as

$$H_{\text{sd}} = \sum_{t=1}^{8760} \mathbb{I}\left(D_t^{\text{unmet}} > \varepsilon\right), \tag{13}$$

and then expressed in day-equivalent units:

$$D_{\text{sd}}^{\text{eq}} = \frac{H_{\text{sd}}}{24}. \tag{14}$$

Unlike a calendar-day shortage count, ESD can be fractional because it represents the cumulative number of shortage hours divided by 24. The annual unused-PV ratio is

$$\text{Unused}\% = 100 \frac{\sum_t P_t^{\text{unused}}}{\sum_t P_t^{\text{PV}}}. \tag{15}$$

The net present value (NPV) of the system is

$$\text{NPV}(\mathbf{x}) = C_{\text{inv}}(\mathbf{x}) + \sum_{y=1}^{N} \frac{C_{\text{O\&M},y}(\mathbf{x}) + C_{\text{rep},y}(\mathbf{x})}{(1+r)^y}, \tag{16}$$

and the cost of water is

$$\text{COU}(\mathbf{x}) = \frac{\text{NPV}(\mathbf{x})}{V_{\text{delivered}}(\mathbf{x})}. \tag{17}$$

ARTICLE IN PRESS

The penalty-augmented objective is

$$J(\mathbf{x}) = \mathrm{COU}(\mathbf{x}) + \alpha \max(0, \mathrm{LLP}(\mathbf{x}) - \mathrm{LLP}_{\max}) + \beta \max(0, D_{\mathrm{sd}}^{\mathrm{eq}}(\mathbf{x}) - D_{\mathrm{sd,max}}^{\mathrm{eq}}). \tag{18}$$

The nominal reliability limits are $\mathrm{LLP}_{\max} = 0.010$ and $D_{\mathrm{sd,max}}^{\mathrm{eq}} = 5$ days/year. Penalty coefficients are $\alpha = 100$ and $\beta = 0.1$. A tightening to $\mathrm{LLP}_{\max} = 0.008$ is used only for the robustness-margin design, not as the nominal design requirement. Table 2' values define the cost model used to calculate NPV and COU for all nominal and robustness-margin designs.

Table 2: Baseline economic parameters used in the techno-economic assessment.

Parameter	Symbol / basis	Value	Unit / rule
PV module unit cost	c_{PV}	1.00	\$/W
MPPT cost	C_{MPPT}	411	\$
Pump cost	C_{pump}	800	\$
Reservoir cost	C_{tank}	$20(V/1000) + 75$	\$, with V in L
Annual O&M cost	$C_{\mathrm{O\&M}}$	50	\$/year
Labour price coefficient	k_{lab}	0.07	–
Real discount rate	r	0.10	–
PV lifetime	L_{PV}	20	years
MPPT lifetime	L_{MPPT}	10	years
Pump lifetime	L_{pump}	10	years

2.5. Optimization validation, integer handling, and robustness tests

The decision vector is $\mathbf{x} = [S, P, V_{\max}]$, where S and P are the integer PV configuration variables and $V_{\max}$ is the tank capacity. In the implemented model, the admissible design ranges are $S \in \{2, \ldots, 12\}$, $P \in \{1, \ldots, 4\}$, and $V_{\max} \in [5, 30]$ m^3. An exploratory GWO search is used as a derivative-free search tool, but the final global-optimality interpretation is not based on a single GWO trajectory. Instead, an enumeration-refined check is applied over the admissible integer (S, P) combinations and a tank-capacity grid, followed by local refinement around feasible boundary regions. This provides a direct consistency check for the reported optimum and separates final design selection from random design-space visualization.

For the GWO implementation, real-valued updates are mapped to the nearest admissible integers for S and P and then clipped to their bounds. Because such mapping can affect metaheuristic search directionality, the final design selection is based on the enumeration-refined feasible optimum rather than on the rounded GWO trajectory alone. The random/Pareto scan is therefore used only as a design-space visualization tool and not as the final optimizer.

Robustness is assessed by perturbing demand in two stages. For each Monte Carlo realization, a multiplicative scaling factor is sampled as $\zeta \sim \mathcal{U}(0.85, 1.15)$, and hour-to-hour variability is represented by $\epsilon_t \sim \mathcal{N}(0, 0.20^2)$ through the bounded multiplicative factor $\eta_t = \mathrm{clip}(1 + \epsilon_t, 0.2, 2.0)$. The uncertain hourly demand is therefore represented as $D_t^{\mathrm{MC}} = D_t\, \zeta\, \eta_t$. The nominal designs are first tested under this uncertainty model. A robustness-margin design is then generated by tightening the nominal target to $\mathrm{LLP}_{\max} = 0.008$ before applying the same Monte Carlo test. This procedure is intended to evaluate mean-robust behavior; it is not claimed to satisfy strict high-percentile chance-constrained feasibility.

To directly test optimizer reliability, a computationally constrained multi-seed re-check was carried out on the S1 reference scenario (the same scenario used for the PV- and tank-capacity sweeps in Figures 7 and 8). Because a single full 8760-h evaluation of the coupled PV–pump–tank model requires on the order of 15–16 s on the available hardware, the budget for this targeted check was necessarily small: five independent seeds each for GWO and PSO

ARTICLE IN PRESS

at $N_{\text{pop}} = 4$, $T_{\max} = 3$ (12 evaluations per run), three seeds for each of three integer-mapping rules, and two seeds across a 2×2 α–β grid for the static-versus-adaptive penalty comparison (Table 3; Figure 3). Each row in Table 3 summarizes independent seeds (or seed×configuration combinations) evaluated with the full 8760-h simulation model; "feasible" denotes LLP ≤ 0.010.

At this reduced budget, only 2 of 5 GWO seeds and 2 of 5 PSO seeds reached a feasible design. Across the five GWO runs, LLP ranged from 0.0062 to 0.1199 and COU from 1.537 to 2.319 \$/m^3, whereas the five PSO runs produced an even wider LLP range of 0.0022–0.2467 and a COU range of 1.615–2.152 \$/m^3. This substantial seed-to-seed dispersion confirms the instability expected from a small-population, few-iteration metaheuristic search. Among the integer-mapping rules, nearest-neighbor repair coincided numerically with simple rounding on this unit-spaced (S, P) grid, whereas stochastic floor/ceil mapping produced a narrower LLP spread (0.0132–0.0468). For the penalty formulation, the static scheme was insensitive to the tested $\alpha \in \{50, 200\}$ and $\beta \in \{0.05, 0.5\}$ values at this budget, whereas switching to an iteration-scaled adaptive penalty changed the outcome for one of the two seeds by converting an infeasible trajectory into a feasible one. Taken together, these reduced-budget diagnostics explain why the enumeration-refined search (Section 3.1), rather than any single small-budget metaheuristic run, is used as the primary optimizer-validation evidence across all four scenarios. A larger-budget, all-scenario version of this multi-seed re-check is identified as future work in Section 4.

Table 3: Reduced-scope, computationally constrained optimizer-robustness re-check on the S1 reference scenario.

Configuration	Runs	Feasible	LLP range	COU range (\$/m^3)
GWO (N_{pop}=4, $T_{\max}$=3)	5	2	0.0062–0.1199	1.537–2.319
PSO (swarm=4, iters=3)	5	2	0.0022–0.2467	1.615–2.152
Integer: round	3	0	0.0117–0.1199	1.537–1.996
Integer: floor/ceil (stochastic)	3	0	0.0132–0.0468	1.671–1.920
Integer: repair (nearest)	3	0	0.0117–0.1199	1.537–1.996
Penalty: static (α, β fixed)	8	0	0.0117–0.0366	1.690–1.996
Penalty: adaptive (iteration-scaled)	8	4	0.0064–0.0703	1.690–2.022

Note: For the optimizer and integer-mapping rows, "Runs" and "Feasible" denote independent seeds. For the penalty rows, they denote seed–parameter evaluations (2 seeds × 4 α–β settings = 8); therefore, the four feasible adaptive-penalty evaluations do not represent four independent feasible seeds.

ARTICLE IN PRESS

ARTICLE IN PRESS

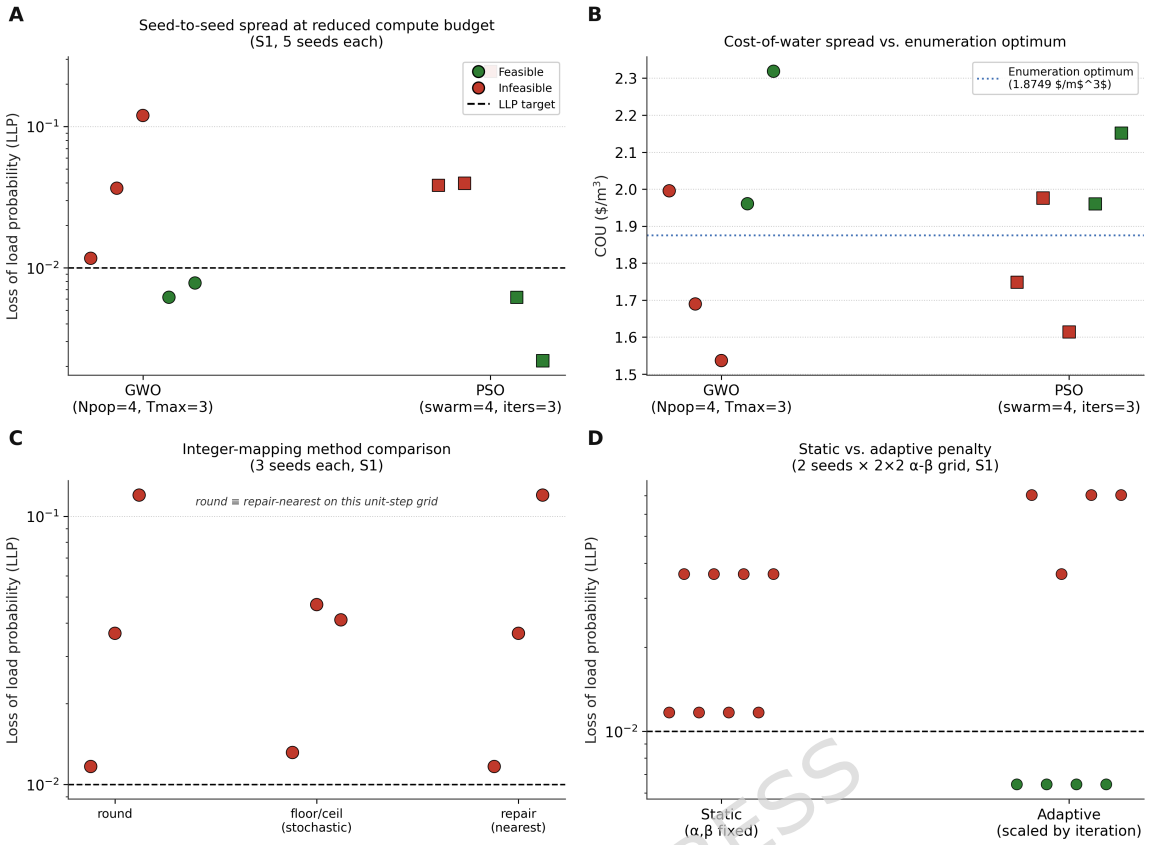


Figure 3: Reduced-scope optimizer-robustness re-check for the S1 reference scenario. (A)–(B) GWO and PSO show substantial seed-to-seed LLP variation and 40% feasibility across five runs. (C) Nearest-neighbor repair matches simple rounding, while stochastic floor/ceil mapping reduces the LLP spread. (D) The static penalty is insensitive to the tested α–β range, whereas the adaptive penalty changes one of the two seed outcomes.

Additional sensitivity analyses quantify the effects of (i) seasonal demand redistribution with preserved annual water volume, (ii) static-head increases representing possible groundwater drawdown, (iii) uncovered-tank evaporation, (iv) pump-efficiency degradation, (v) generic transient PV-to-pump power loss representing unresolved sub-hourly interruptions, and (vi) S4 pulse-window flow adequacy. These tests are designed to expose the fragility of just-feasible boundary designs rather than to replace a full hydrogeological or sub-hourly dynamic model.

The workflow is summarized in Figure 4. The physical model and scenario-based annual simulation provide the performance indicators used in the exploratory GWO search. The best GWO candidate is subsequently checked through an enumeration-refined feasible search to obtain the validated nominal design. A reliability-margin design is then generated by tightening the nominal LLP constraint, and both the nominal and margin designs are evaluated under demand uncertainty, seasonal redistribution, and physical stress conditions.

3. Results and Discussion

3.1. Optimization verification and enumeration-refined nominal designs

Figure 5 illustrates the rapid stabilization of the exploratory GWO search and is used as an optimizer-diagnostics plot. Final design selection is independently verified using the enumeration-refined comparison in Figure 6 and Table 4. The multi-panel figure combines the S1 feasible design-space landscape, the GWO–enumeration cost comparison, and the

ARTICLE IN PRESS

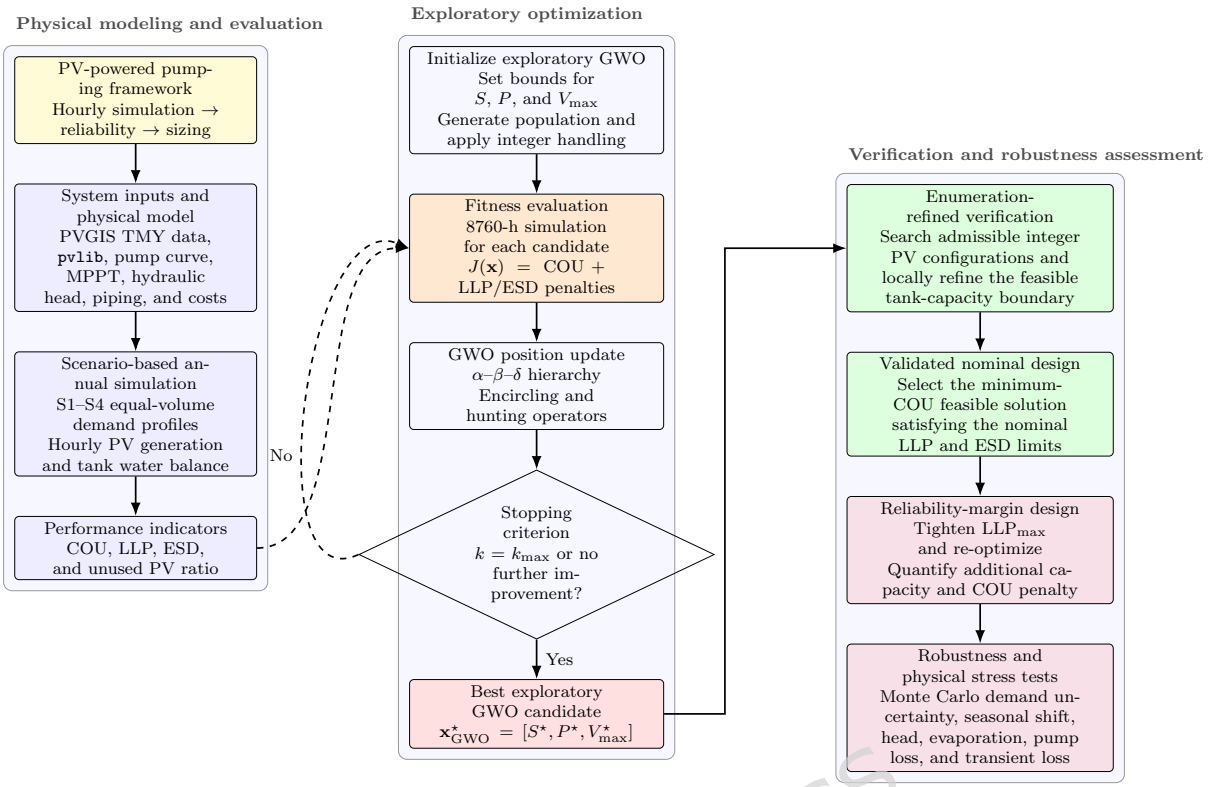


Figure 4: Proposed simulation–optimization, verification, and robustness-assessment workflow.

resulting capacity adjustments. This comparison separates the random design-space scan from final design selection and shows that the enumeration-refined S3 feasible design differs from the exploratory GWO candidate reported in Table 4.

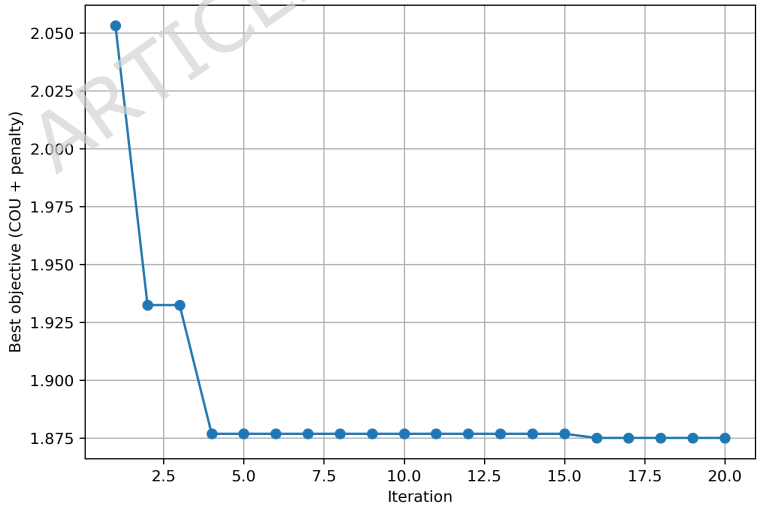


Figure 5: Convergence history of the exploratory Grey Wolf Optimizer for the S1 baseline scenario.

The first results step verifies whether the GWO-identified optima are consistent with the mixed-integer design space. Figure 6 summarizes the comparison between the GWO-reported designs and the enumeration-refined feasible solutions. The refined search confirms the S1, S2, and S4 designs to within a negligible COU difference, but it identifies a lower-cost S3 feasible design with a 10×3 PV configuration rather than the 8×4 configuration found by the exploratory search. This distinction is important because it demonstrates that

ARTICLE IN PRESS

the near-boundary objective surface is relatively flat and partly shaped by integer module combinations.

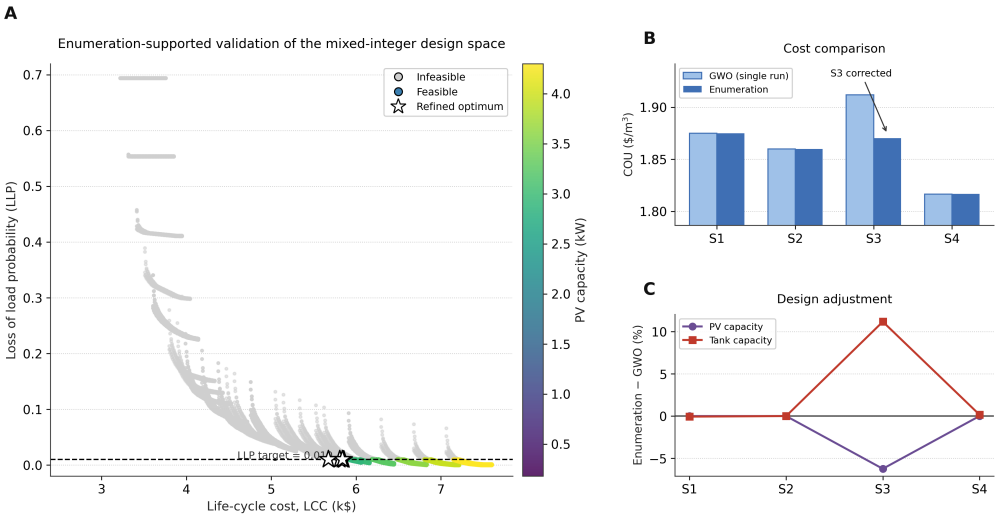


Figure 6: Enumeration-supported validation of mixed-integer sizing results.

Table 4: Enumeration-refined validation of the nominal optima.

Scenario	Enumeration PV (kW)	Enumeration tank (m^3)	Enumeration COU ($/$m^3$)	GWO COU ($/$m^3$)	ΔCOU ($/$m^3$)	Note
S1	2.70	29.30	1.875	1.875	0.000	Consistent
S2	2.70	27.10	1.860	1.860	0.000	Consistent
S3	2.70	28.60	1.870	1.912	−0.042	Lower-cost feasible design
S4	2.52	29.80	1.817	1.817	0.000	Refined feasible boundary

The enumeration-refined nominal optima are reported in Table 5. The table presents the cost-minimal boundary designs satisfying both the LLP and ESD constraints under nominal demand. The optimal PV capacities lie in the narrow range of 2.52–2.70 kW. This should be interpreted as confirmation that, under the equal-daily-volume assumption and the adopted 90 W module discretization, all scenarios share a similar annual energy floor; it should not be over-interpreted as a general discovery independent of demand magnitude, site, or module granularity.

Table 5: Enumeration-refined nominal designs under the deterministic demand profiles.

Scenario	S	P	PV (kW)	Tank (m^3)	LLP –	ESD (d/y)	COU ($/$m^3$)
S1 Uniform	10	3	2.70	29.30	0.00991	3.88	1.875
S2 Morning-only	10	3	2.70	27.10	0.00998	1.08	1.860
S3 Split morning–evening	10	3	2.70	28.60	0.00998	1.79	1.870
S4 Greenhouse pulsed	7	4	2.52	29.80	0.00997	1.63	1.817

Relative to S1, S2 reduces ESD by approximately 72% while reducing tank volume by 7.5% and COU by 0.8%. In the enumeration-refined solution, S3 uses the same 2.70 kW PV capacity as S1 and S2, reduces ESD by approximately 54%, and slightly lowers COU relative to S1. S4 achieves the lowest COU, approximately 3.1% below S1, with a smaller PV capacity but a slightly larger tank. Thus, the interpretation is deliberately moderate: demand timing

ARTICLE IN PRESS

strongly affects shortage duration and storage-recovery signatures, but it does not eliminate the need for a similar minimum PV energy floor.

The single-parameter diagnostic plots help explain the physical transition from energy-limited to storage-limited operation. Figure 7 shows that increasing installed PV capacity sharply reduces both LLP and ESD up to the feasibility region, after which additional PV capacity provides only marginal reliability improvement. Figure 8 shows the complementary storage-controlled transition at fixed PV capacity. In both figures, the red duration axis represents ESD rather than a count of calendar days containing shortage. The tank-capacity diagnostic also shows the diminishing reliability return from additional storage once diurnal buffering is sufficient.

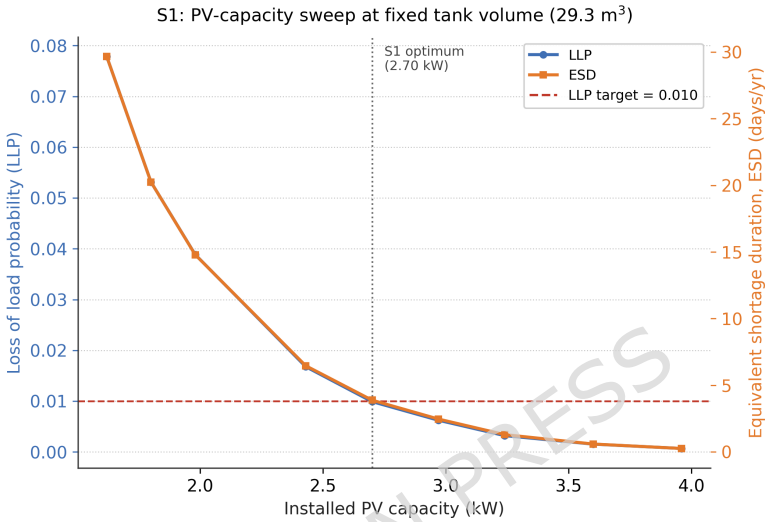


Figure 7: Variation of LLP and ESD, where ESD is computed as the shortage hours divided by 24, with installed PV capacity under the S1 diagnostic sweep.

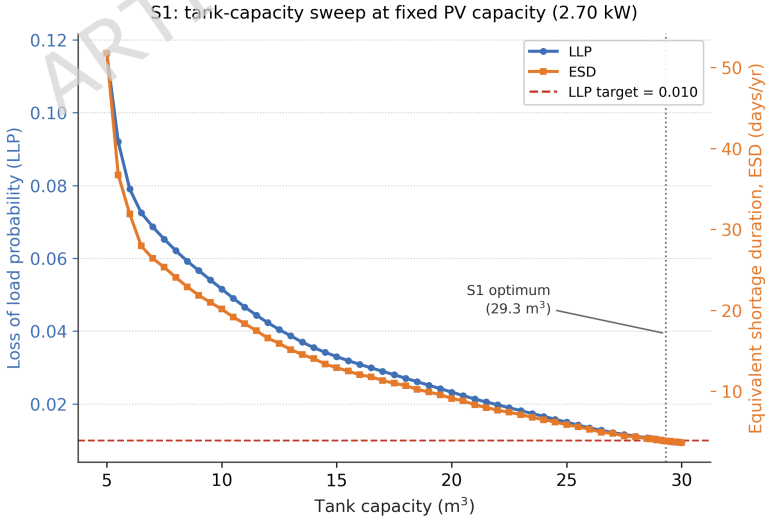


Figure 8: Variation of LLP and ESD with tank capacity at fixed PV capacity.

The representative operating profiles in Figure 9 provide a physical explanation of simultaneous noon curtailment and night-time water stress by showing storage saturation, midday curtailment, and night-time depletion. Tank saturation and pump-off logic may create operational cycling that is not fully resolved at hourly resolution; this issue is addressed in the limitations and through transient-loss sensitivity.

ARTICLE IN PRESS

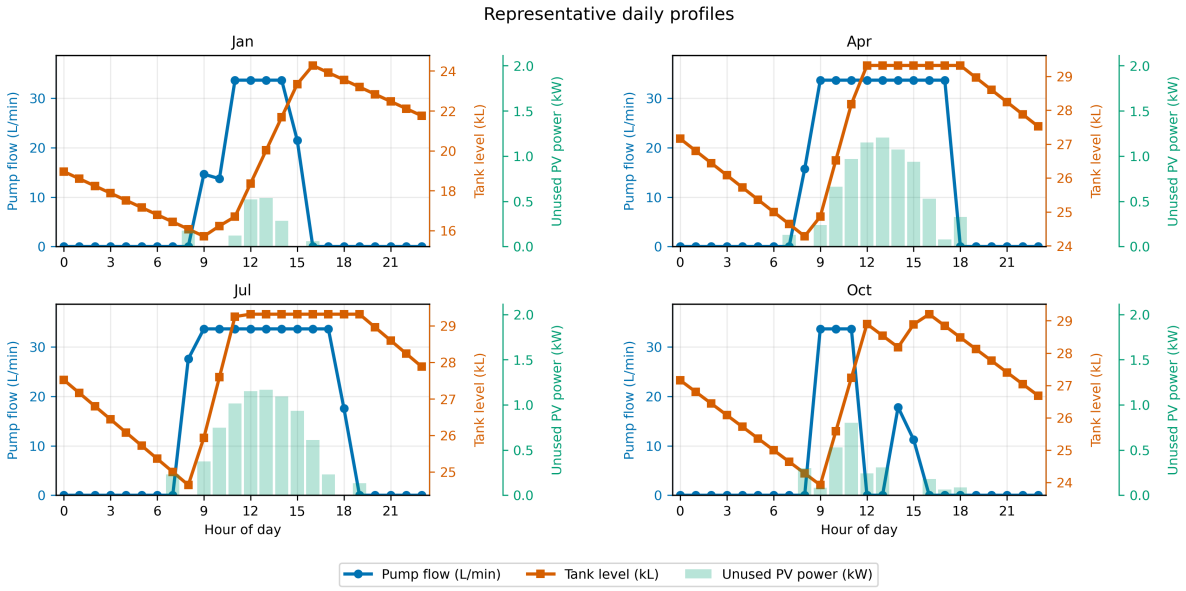


Figure 9: Representative daily profiles of pump flow, tank level, and unused PV power under uniform demand.

Figure 10 is a random/Pareto-style design-space scan showing feasibility clustering and discrete component effects; it is not the optimizer used to obtain the designs in Table 5. The figure illustrates the reliability–investment threshold and the discrete clustering induced by integer PV-module combinations, whereas the final reported optima are obtained from the enumeration-refined search.

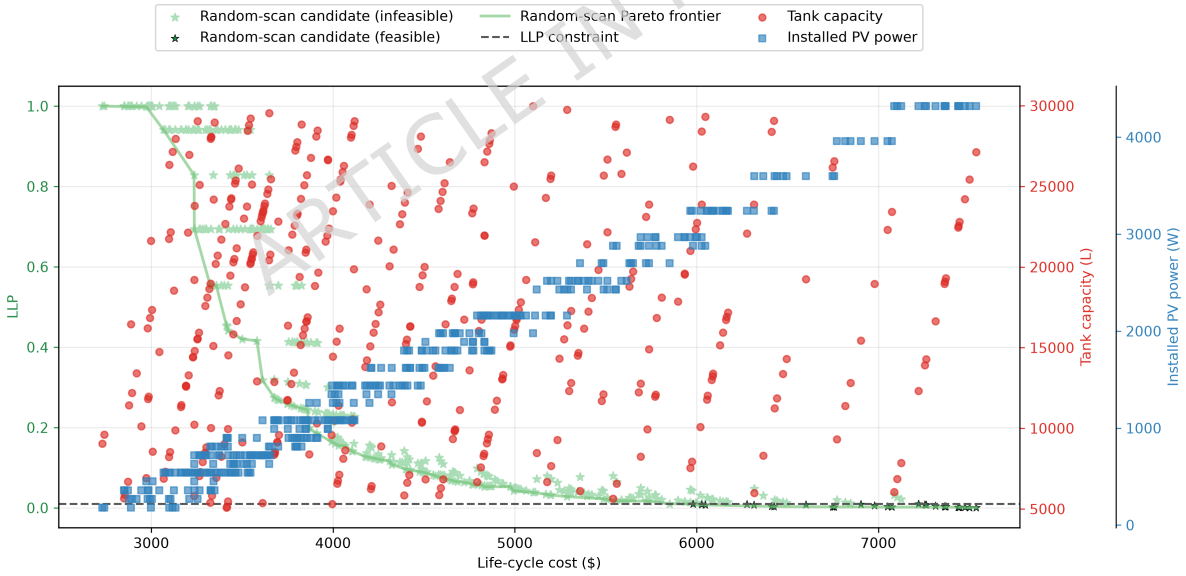


Figure 10: Random-scan LCC–LLP design-space visualization for Scenario S1.

3.2. Nominal boundary designs and robustness-margin sizing

Monte Carlo testing reveals that deterministic boundary designs are sensitive to demand uncertainty. As shown in Table 6 and Figure 11, the nominal designs satisfy the deterministic LLP target but their Monte Carlo mean LLP exceeds 0.010 in all scenarios. The margin designs in Table 6 reduce the Monte Carlo mean LLP below the 0.010 target, but the 95th-percentile LLP remains above 0.010; therefore, they should be interpreted as mean-robust designs rather than strict chance-constrained solutions. Panels (A) and (B) in Figure 11 show that tightening the nominal LLP target from 0.010 to 0.008 reduces the Monte Carlo mean

ARTICLE IN PRESS

LLP below the 0.010 target for all scenarios, while the 95th-percentile LLP remains above the strict target. Panels (C) and (D) quantify the associated COU penalty and the capacity adjustments needed to obtain the margin. This confirms that a cost-minimal just-feasible design should not be presented as robustly feasible under uncertain demand. To quantify a practical margin, the nominal LLP target was tightened from 0.010 to 0.008 and the resulting designs were tested under the same uncertainty model.

Table 6: Nominal boundary designs and robustness-margin designs under Monte Carlo demand uncertainty.

Scenario	Design	PV (kW)	Tank (m^3)	Nominal LLP –	Nominal COU ($/$m^3$)	MC mean LLP –	MC95 LLP –	MC mean ESD (d/y)
S1	Nominal, $LLP_{max} = 0.010$	2.70	29.30	0.00991	1.875	0.01045	0.02043	4.06
S1	Margin, $LLP_{max} = 0.008$	2.88	28.50	0.00792	1.927	0.00802	0.01546	3.14
S2	Nominal, $LLP_{max} = 0.010$	2.70	27.10	0.00998	1.860	0.01098	0.02078	1.27
S2	Margin, $LLP_{max} = 0.008$	2.88	27.00	0.00771	1.916	0.00787	0.01483	0.91
S3	Nominal, $LLP_{max} = 0.010$	2.70	28.60	0.00998	1.870	0.01069	0.02049	1.93
S3	Margin, $LLP_{max} = 0.008$	2.88	28.00	0.00783	1.924	0.00796	0.01539	1.45
S4	Nominal, $LLP_{max} = 0.010$	2.52	29.80	0.00997	1.817	0.01121	0.02373	1.82
S4	Margin, $LLP_{max} = 0.008$	2.70	28.50	0.00793	1.866	0.00824	0.01747	1.35

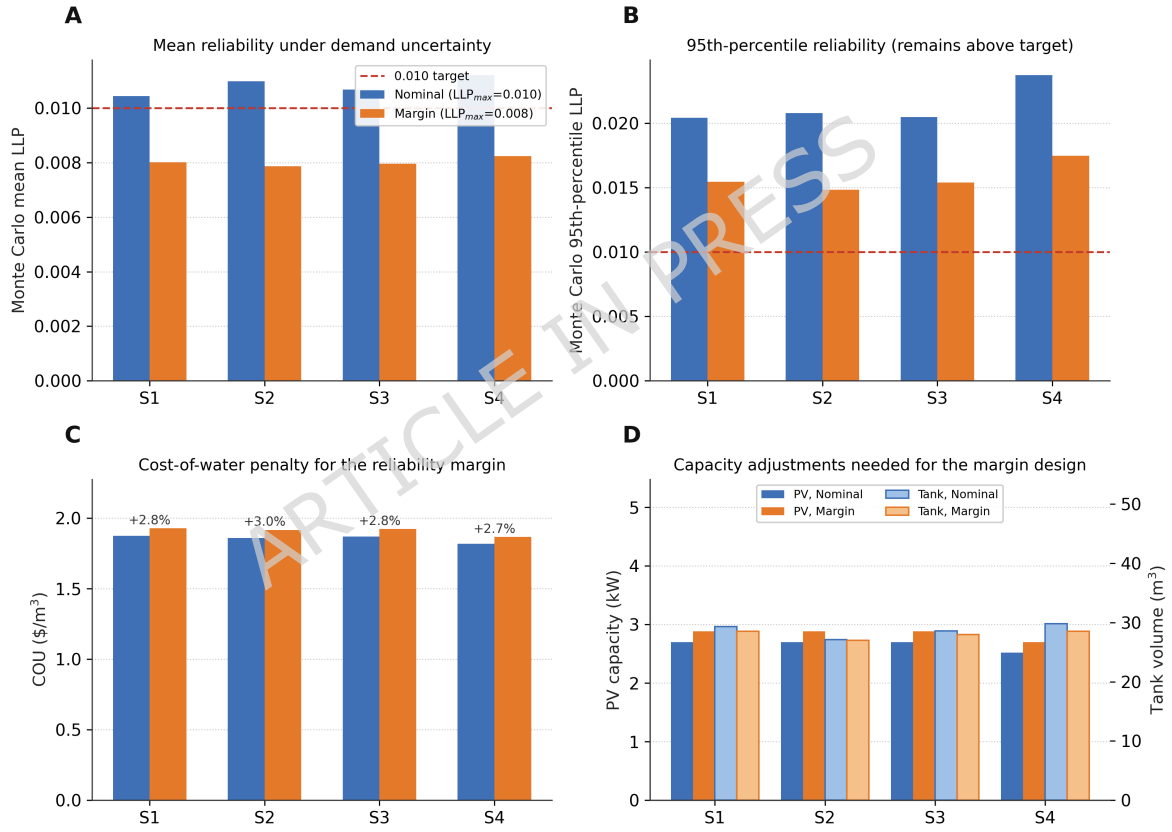


Figure 11: Effect of the robustness-margin design on Monte Carlo reliability.

The robustness-margin results change the design interpretation. The deterministic optima are best viewed as cost-minimal boundary solutions for nominal demand, whereas the margin designs are more suitable when average reliability under demand uncertainty is required. The 95th-percentile LLP values remain above 0.010 even for the margin designs, indicating that strict chance-constrained feasibility would require a more conservative reliability target, larger storage, additional PV capacity, adaptive scheduling, or backup flexibility. This distinction is central to the conclusions.

ARTICLE IN PRESS

3.3. Seasonal demand redistribution

The results show that seasonal demand–generation co-variation can substantially reduce LLP and ESD for the same nominal hardware configuration (see Table 7). Real irrigation demand is seasonal and often correlated with solar availability. To isolate this effect without changing total annual water volume, two annual-volume-preserving seasonal redistribution cases are evaluated and visualized in Figure 12. The figure shows that shifting demand toward high-resource months substantially reduces LLP and ESD without changing the total annual water requirement, confirming that the fixed-daily-demand baseline is a controlled but conservative diagnostic case. The mild and strong cases shift a larger share of annual demand toward months with higher solar availability while preserving the same annual water requirement.

Table 7: Seasonal demand-redistribution sensitivity with annual water volume preserved.

Scenario	Baseline LLP –	Baseline ESD (d/y)	Mild LLP –	Mild ESD (d/y)	Strong LLP –	Strong ESD (d/y)
S1	0.00991	3.88	0.00241	1.17	0.00057	0.29
S2	0.00998	1.08	0.00283	0.29	0.00079	0.08
S3	0.00998	1.79	0.00262	0.54	0.00039	0.08
S4	0.00997	1.63	0.00291	0.58	0.00041	0.13

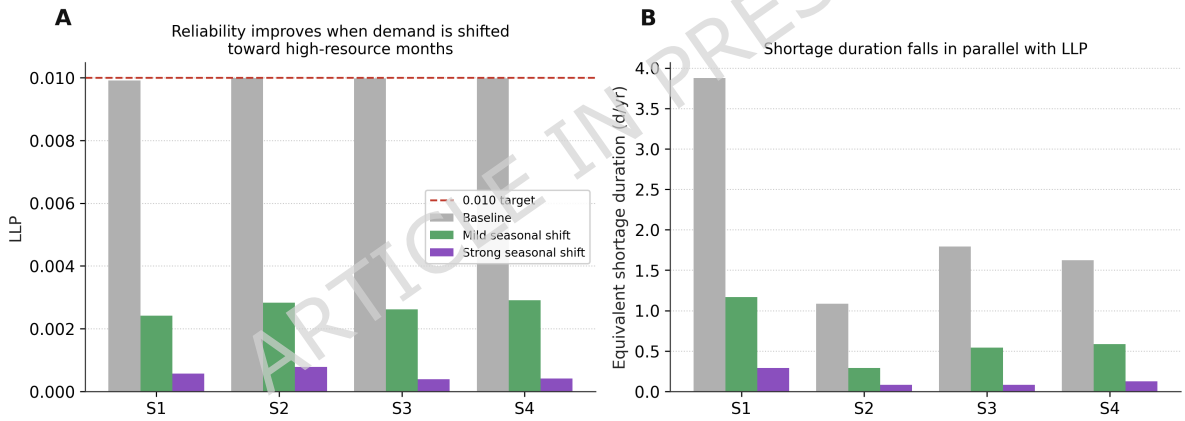


Figure 12: Seasonal demand-redistribution sensitivity under annual-volume-preserving irrigation demand.

These results show that the fixed-daily-demand baseline is a deliberately controlled but conservative diagnostic setting. When seasonal irrigation demand is shifted toward high-resource months while annual demand is preserved, both LLP and ESD decline markedly. This supports the broader conclusion that temporal alignment is important, but it also narrows the generality of the equal-daily-volume assumption: crop-specific evapotranspiration, soil moisture feedback, and seasonal water allocations should be incorporated before site-level deployment.

3.4. Physical sensitivity analyses

Several physical assumptions were perturbed to assess whether the nominal boundary designs remain reliable under plausible deviations from the baseline model. Table 8 and Figure 13 summarize the effects of a 5 m increase in static head, 2 mm/day evaporation from an uncovered tank, 10% pump-efficiency degradation, and an additional 2% PV-to-pump power derating representing unresolved transient losses. Table 8 reports the corresponding absolute

ARTICLE IN PRESS

LLP values for each nominal design. Values above 0.010 indicate violation of the nominal reliability target. Figure 13 presents the same results as ratios relative to the 0.010 LLP target, with the corresponding absolute LLP values shown in parentheses. Ratios greater than 1.00 therefore indicate that the tested perturbation causes the nominal reliability constraint to be violated. Overall, the just-feasible boundary designs are sensitive to all four perturbations, with static-head increase and pump-efficiency degradation producing the largest reliability deterioration.

Table 8: Absolute LLP values of the nominal boundary designs under selected physical perturbations.

Scenario	Baseline	+5 m head	2 mm/day evaporation	10% pump-efficiency loss	2% transient loss
S1	0.00991	0.02064	0.01003	0.01436	0.01049
S2	0.00998	0.02129	0.01009	0.01495	0.01051
S3	0.00998	0.02095	0.01011	0.01461	0.01056
S4	0.00997	0.02542	0.01006	0.01825	0.01045

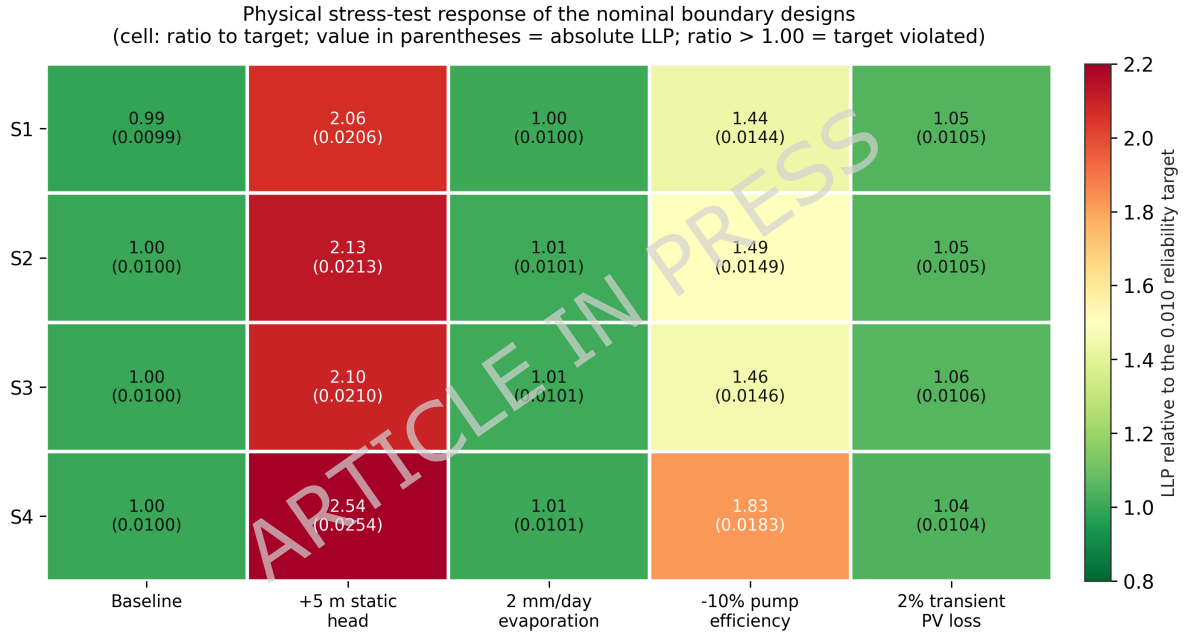


Figure 13: Physical stress-test response of the nominal boundary designs. Each cell reports the LLP ratio relative to the 0.010 reliability target, with the corresponding absolute LLP shown in parentheses. Ratios above 1.00 indicate violation of the nominal reliability constraint.

The static-head sensitivity confirms that neglecting groundwater-level variation can materially underestimate the pumping-energy requirement and overestimate system reliability. A 5 m increase in static head causes all nominal designs to exceed the LLP target. The evaporation sensitivity indicates that the baseline results should be interpreted as representative of covered or evaporation-minimized storage; uncovered tanks in semi-arid environments require an additional reliability margin. The pump-efficiency and transient-loss tests further indicate that an hourly model may overestimate practical reliability when equipment degradation, start–stop cycling, or short-duration irradiance fluctuations are not explicitly resolved.

For S4, the pulse-window diagnostic separately examines whether the remaining shortages are caused by an instantaneous flow-capacity limitation. The peak hourly demand is 1080 L/h, whereas the maximum simulated pump inflow is approximately 2020 L/h. The

ARTICLE IN PRESS

modeled shortage is therefore not caused by peak demand exceeding the available pump-flow capacity. Instead, it occurs when high-demand pulse windows coincide with depleted storage and insufficient concurrent inflow in the hourly water balance. Because no separate outlet-flow or distribution-network constraint is included, this result should be interpreted as an hourly storage–inflow adequacy limitation rather than as a detailed hydraulic-network failure.

3.5. Tank-state reliability interpretation

The tank-state perspective remains a useful diagnostic and is interpreted as follows. Under uniform demand, the tank primarily bridges night-time and multi-day depletion periods. Under morning-only and split demand, the tank supports diurnal recovery and reduces the duration of shortage exposure. Under S4, the tank has a dual role: the optimized capacity still represents a multi-day water reserve relative to the 8.64 m^3/day baseline demand, while the remaining shortage events occur during pulse windows when storage is depleted or concurrent inflow is insufficient. Therefore, S4 should not be characterized as only a short-term buffer.

The tank-state and hourly-shortage figures connect annual scalar metrics to time-resolved physical failure signatures. Figure 14 shows how LLP and ESD vary with tank capacity across demand topologies, while Figure 15 shows that similar annual LLP levels can correspond to distinct shortage timing patterns. The maps demonstrate that annual LLP values can hide fundamentally different failure-time distributions. Figure 16 distinguishes peak-flow feasibility from storage-state-driven shortage: the peak hourly demand does not exceed the maximum modeled pump inflow, while remaining unmet demand appears when pulse windows coincide with low stored volume and insufficient concurrent inflow.

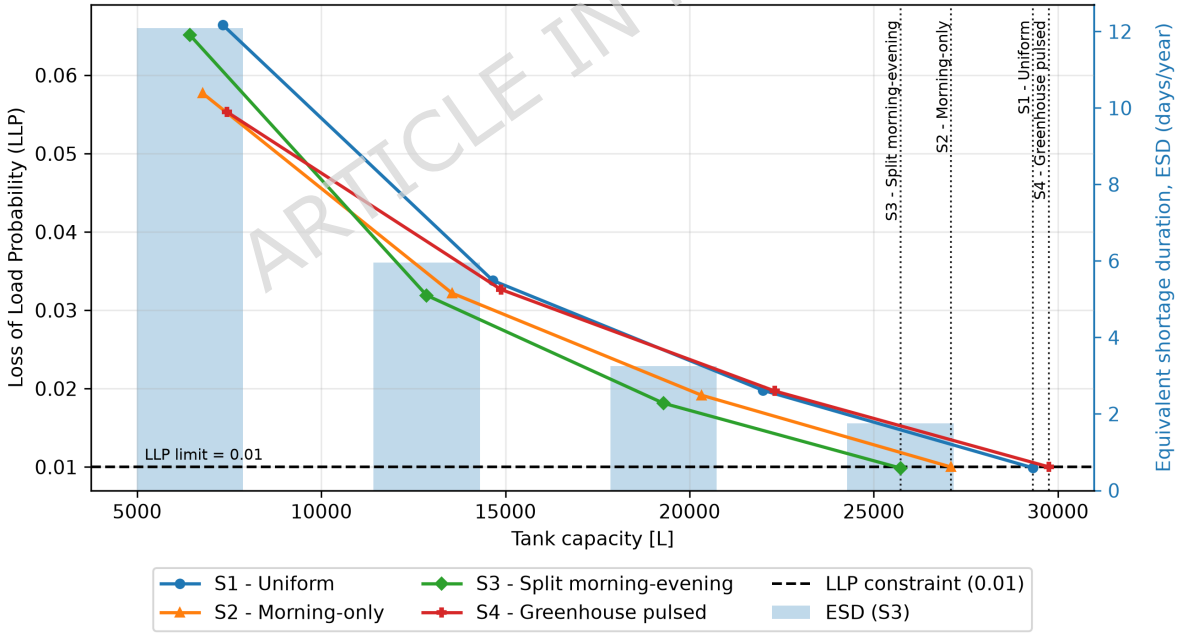


Figure 14: Tank-capacity diagnostic for Scenarios S1–S4. The left axis shows LLP for all scenarios, whereas the right axis presents the ESD diagnostic for Scenario S3. The LLP threshold identifies the storage-dependent feasibility transition.

ARTICLE IN PRESS

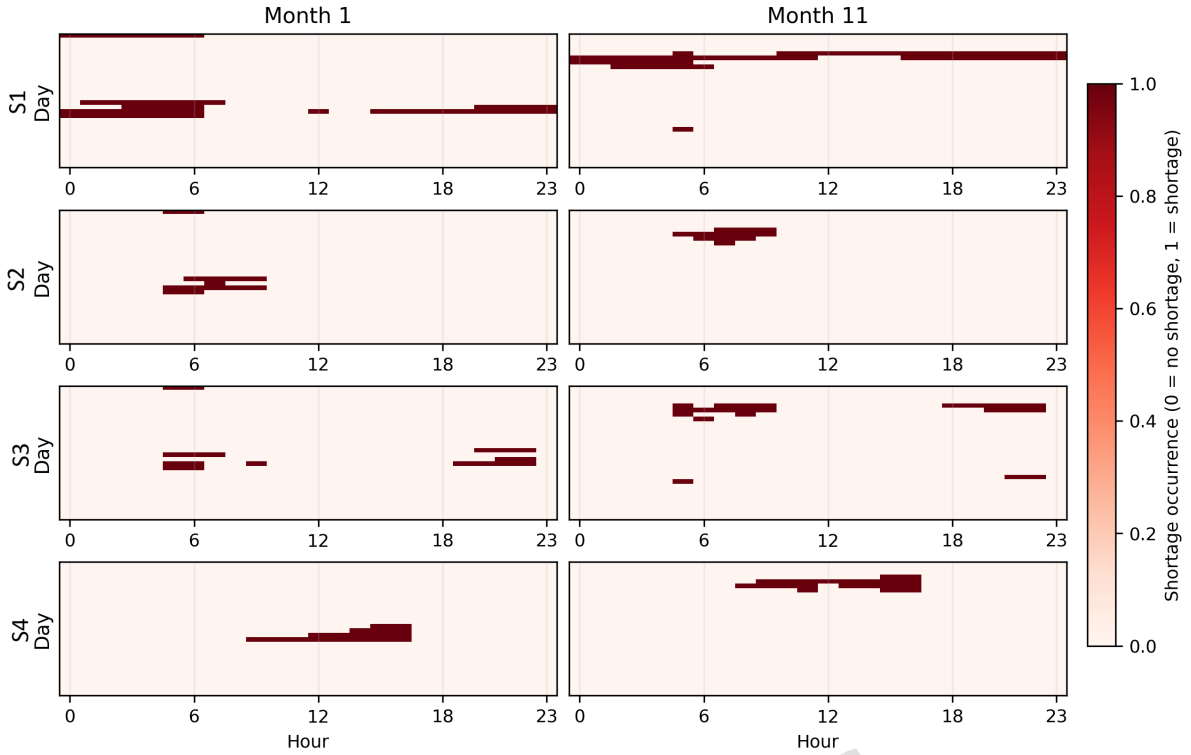


Figure 15: Representative hourly shortage-occurrence maps for Months 1 and 11 under the nominal configurations of Scenarios S1–S4.

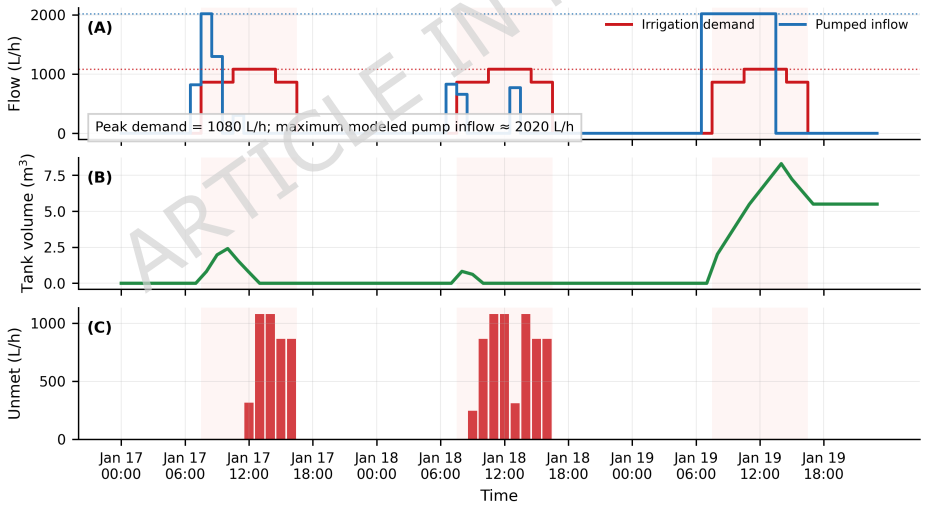


Figure 16: S4 pulse-window diagnostic.

Together, these results support a more cautious conclusion: irrigation timing is an important operational co-design factor for shortage duration, tank recovery, and curtailment interpretation, but it does not replace robust hydraulic design, site-specific groundwater assessment, or uncertainty-aware capacity margins.

4. Limitations and Future Research Directions

The study has several limitations that define the scope of interpretation. First, the case study is restricted to a single location, one representative daily water demand level, and one cost dataset. The quantitative sizing values should therefore not be generalized without local

ARTICLE IN PRESS

recalibration. Second, the equal-daily-volume demand scenarios are diagnostic profiles rather than field-measured irrigation schedules. They isolate intra-day timing effects, but they do not replace crop-specific evapotranspiration, soil-moisture feedback, or adaptive precision-irrigation control. Third, the baseline model uses a fixed static head and therefore does not simulate transient aquifer drawdown, cone-of-depression dynamics, or aquifer recovery. The added head sensitivity shows that this omission can materially affect reliability. Fourth, the baseline reservoir assumes covered or evaporation-minimized storage; uncovered storage in semi-arid climates requires additional margin. Fifth, the hourly resolution cannot resolve sub-hourly cloud passages, MPPT instability, high-frequency start–stop cycling, or mechanical wear due to pump cycling. Replacement costs are therefore not adjusted for cycling-induced degradation. Sixth, the robustness-margin design improves mean Monte Carlo reliability but does not guarantee strict high-percentile chance-constrained feasibility. Seventh, the multi-seed GWO/PSO re-check, integer-mapping comparison, and penalty-formulation comparison reported in Section 2.5 were themselves computationally constrained (5 seeds at $N_{pop} = 4$, $T_{max} = 3$, on the S1 reference scenario only), because a single full 8760-h model evaluation takes 15–16 s on the available hardware; the enumeration-refined check therefore remains the primary optimizer-validation evidence for all four scenarios, and a larger-budget, all-scenario multi-seed/PSO study is left for a dedicated follow-up computational effort. Future work should integrate stochastic or chance-constrained optimization, dynamic groundwater models, crop-specific seasonal demand, finer temporal resolution, pump-cycling degradation models, secondary dispatchable loads or demand-response mechanisms to utilize curtailed PV energy, and the larger-budget optimizer benchmarking noted above.

5. Conclusion

This study evaluated standalone PVWPS sizing under four intra-day irrigation demand topologies and integrated optimization verification, robustness-margin testing, seasonal-demand sensitivity, and physical-sensitivity checks. Enumeration-refined nominal designs satisfied the deterministic LLP target with PV capacities between 2.52 and 2.70 kW and storage volumes between 27.10 and 29.80 m^3. Under the equal-daily-volume assumption, this narrow PV range confirms a common annual energy floor shaped by the adopted module discretization and demand magnitude, while demand timing primarily affects storage use and shortage duration. Relative to uniform demand, morning-only, split morning–evening, and greenhouse-pulsed profiles reduced equivalent shortage duration by approximately 72%, 54%, and 58%, respectively. Cost differences were more moderate: the greenhouse-pulsed case achieved the lowest COU, approximately 3.1% below the uniform-demand case. These findings support treating irrigation timing as an important operational co-design factor, but not as a substitute for adequate PV and storage sizing.

Monte Carlo testing showed that nominal just-feasible designs are not robustly feasible on average under demand uncertainty. A robustness-margin design obtained by tightening the nominal LLP target to 0.008 reduced mean Monte Carlo LLP below 0.010 for all scenarios, although the 95th-percentile LLP remained above the target. Thus, uncertainty-aware deployment requires explicit design margins or stricter chance-constrained optimization. Additional sensitivity tests showed that a 5 m increase in static head, uncovered-tank evaporation, pump-efficiency degradation, and transient PV-to-pump losses can all push boundary designs beyond the reliability target. The practical implication is that cost-minimal nominal designs should be used as reference boundary solutions, whereas field deployment in groundwater-dependent semi-arid regions should include robustness margins, seasonal demand modeling, and site-specific hydraulic validation.

ARTICLE IN PRESS

Funding

This research did not receive any specific grant from funding agencies in the public, commercial, or not-for-profit sectors.

Code Availability

The version-controlled code, processed inputs, numerical outputs, and analysis files used to generate the results, tables, and figures reported in this study are publicly available at https://github.com/alp-coder/pvwps-time-structured-irrigation.

Data Availability

The processed input data and numerical outputs supporting the findings of this study are publicly available in the accompanying GitHub repository at https://github.com/alp-coder/pvwps-time-structured-irrigation. The meteorological input is derived from the publicly available PVGIS SARAH3 dataset cited in the manuscript.

Competing Interests

The authors declare no competing interests.

ARTICLE IN PRESS

References

[1] A. Elnozahy, M. Abdel-Salam, F. K. Abo-Elyousr, Optimal techno-economic energy coordination of solar pv water pumping irrigation systems, Energy 288 (2024) 129817. doi:10.1016/j.energy.2023.129817.

[2] S. Hilarydoss, Suitability, sizing, economics, environmental impacts and limitations of solar photovoltaic water pumping system for groundwater irrigation-a brief review, Environ. Sci. Pollut. Res. Int. 30 (28) (2023) 71491–71510.

[3] T. Vezin, S. Meunier, L. Quéval, J. A. Cherni, L. Vido, A. Darga, P. Dessante, P. K. Kitanidis, C. Marchand, Borehole water level model for photovoltaic water pumping systems, Applied Energy 258 (2020) 114080. doi:10.1016/j.apenergy.2019.114080.

[4] I. Okakwu, A. Alayande, D. Akinyele, O. Olabode, J. Akinyemi, Effects of total system head and solar radiation on the techno-economics of pv groundwater pumping irrigation system for sustainable agricultural production, Scientific African 16 (2022) e01118. doi:10.1016/j.sciaf.2022.e01118.

[5] S. E. Boukebbous, N. Benbaha, A. Bouchakour, H. Ammar, S. Bouhoun, D. Kerdoun, Experimental performance assessment of photovoltaic water pumping system for agricultural irrigation in semi-arid environment of sebseb—ghardaia, algeria, International Journal of Energy and Environmental Engineering 13 (2021). doi:10.1007/s40095-021-00435-8.

[6] K. Kriaa, R. H. Rasheed, M. Shaban, N. S. S. Singh, S. A. Hussein, A. M. Sadeq, K. Hajlaoui, A. Ahmadpour, Techno-economic and environmental evaluation of the performance of a solar water pumping system in arid and desert climates, Scientific Reports 15 (2025) 41576–. doi:10.1038/s41598-025-25505-3.

[7] M. Aliyu, G. Hassan, S. A. Said, M. U. Siddiqui, A. T. Alawami, I. M. Elamin, A review of solar-powered water pumping systems, Renewable and Sustainable Energy Reviews 87 (2018) 61–76. doi:10.1016/j.rser.2018.02.010.

ARTICLE IN PRESS

[8] B. Bouzidi, Reliability and sizing of photovoltaic water pumping systems using loss of power supply probability, Sustainable Energy Technologies and Assessments 4 (2013) 1–10. doi:10.1016/j.seta.2013.08.004.

[9] D. H. Muhsen, T. Khatib, T. E. Abdulabbas, Sizing of a standalone photovoltaic water pumping system using hybrid multi-criteria decision making methods, Solar Energy 159 (2018) 1003–1015. doi:10.1016/j.solener.2017.11.044.

[10] E. E. E. Ahmed, A. Demirci, Multi-stage and multi-objective optimization for optimal sizing of stand-alone photovoltaic water pumping systems, Energy 252 (2022) 124048. doi:10.1016/j.energy.2022.124048.

[11] W. Nemouchi, Y. Amrane, H. Nemouchi, N. L. Boucetta, Energy management for optimal design of pv/wind/diesel system for water pumping irrigation in semi-arid climate, Energy Conversion and Management 304 (2024) 118216. doi:10.1016/j.enconman.2024.118216.

[12] M. Irandoostshahrestani, D. R. Rousse, Photovoltaic electrification and water pumping using the concepts of water shortage probability and loss of power supply probability: A case study, Energies 16 (1) (2023) 1. doi:10.3390/en16010001.

[13] P. Pachaivannan, S. Manimuthu, V. Jegadeesan, Comparative energy performance analysis of solar water pumping systems across diverse climate zones, Journal of Engineering Research 13 (2) (2025) 923–937. doi:10.1016/j.jer.2024.03.011.

[14] N. M. Ahmed, A. M. Hassan, M. A. Kassem, A. M. Hegazi, Y. F. Elsaadawi, Reliability and performance evaluation of a solar pv-powered underground water pumping system, Scientific Reports 13 (1) (2023) 14174. doi:10.1038/s41598-023-41272-5.

[15] K. Karthick, K. Jaiganesh, S. Kavaskar, Comprehensive study, design and economic feasibility analysis of solar pv powered water pumping system, Energy Engineering 118 (6) (2021) 1887–1904. doi:10.32604/EE.2021.017563.

[16] M. Osama, M. Abdel-Salam, A. Elnozahy, Optimization of solar pv water pumping system with different scenarios for storage elements: a case-study in egypt, Environment, Development and Sustainability (2025). doi:10.1007/s10668-025-06949-z.

[17] M. Á. Pardo, R. Cobacho, L. Bañón, Standalone photovoltaic direct pumping in urban water pressurized networks with energy storage in tanks or batteries, Sustainability 12 (2) (2020) 738. doi:10.3390/su12020738.

[18] A. García-Chica, A. M. Rodriguez-Perez, J. J. Caparros-Mancera, C. A. Rodríguez-Gonzalez, R. M. Chica, Integrated photovoltaic system for rainwater collection and sustainable irrigation, Irrigation Science 43 (2025) 1385–1395. doi:10.1007/s00271-025-01028-7.

[19] Y. Anker, B. Doktor, A. Dahan, V. Mirlas, A. Gimburg, S. Petlakh, M. Averbukh, Solar-powered wastewater treatment: Integrating pumped storage and hydroelectric generation for autonomous operation, Energy Reports 14 (2025) 2247–2263. doi:https://doi.org/10.1016/j.egyr.2025.09.003.

[20] D. Li, J. Qu, Y. Mo, Q. Zhu, D. Zhu, Sizing optimization of a stand-alone multi-energy complementary water pumping system for hose-drawn traveler in typical regions of china, Agriculture 16 (2026). doi:10.3390/agriculture16010090.

[21] J. M. Carricondo-Antón, M. A. Jiménez-Bello, J. M. Juárez, A. R. Tomas, P. González-Altozano, Optimization of an isolated photovoltaic water pumping system with technical–economic criteria in a water users association, Irrigation Science 41 (2023) 817–834. doi:10.1007/s00271-023-00859-6.

ARTICLE IN PRESS

ARTICLE IN PRESS

[22] Y. Serbouh, T. Benikhelef, D. Benazzouz, M. A. A. Chikh, S. Touil, A. Richa, H. Mahmoudi, Performance optimization and reliability of solar pumping system designed for smart agriculture irrigation, Desalination and Water Treatment 255 (2022) 4–12. doi:10.5004/dwt.2022.28316.

[23] P. P. Paudel, S. Adhikari, Technical feasibility and economic analysis of solar photovoltaic water pumping system for sustainable irrigation in nepal: a case study, International Journal of Sustainable Engineering 18 (2025) 2590115. doi:10.1080/19397038.2025.2590115.

[24] S. Mirjalili, S. M. Mirjalili, A. Lewis, Grey wolf optimizer, Advances in Engineering Software 69 (2014) 46–61. doi:https://doi.org/10.1016/j.advengsoft.2013.12.007.

[25] M. H. Nadimi-Shahraki, S. Taghian, S. Mirjalili, An improved grey wolf optimizer for solving engineering problems, Expert Systems with Applications 166 (2021) 113917. doi:10.1016/j.eswa.2020.113917.

[26] A. Mazloumi, A. Poolad, M. S. Mokhtari, M. B. Altman, A. Y. Abdelaziz, M. Elsisi, Optimal sizing of a photovoltaic pumping system integrated with water storage tank considering cost/reliability assessment using enhanced artificial rabbits optimization: A case study, Mathematics 11 (2) (2023) 463. doi:10.3390/math11020463.

[27] R. Abbassi, S. Saidi, Design of a novel chaotic horse herd optimizer and application to mppt for optimal performance of stand-alone solar pv water pumping systems, Mathematics 12 (4) (2024) 594. doi:10.3390/math12040594.

[28] Z. Ma, G. Wu, P. N. Suganthan, A. Song, Q. Luo, Performance assessment and exhaustive listing of 500+ nature-inspired metaheuristic algorithms, Swarm and Evolutionary Computation 77 (2023) 101248. doi:10.1016/j.swevo.2023.101248.

[29] A. M. Nassef, M. A. Abdelkareem, H. M. Maghrabie, A. Baroutaji, Review of metaheuristic optimization algorithms for power systems problems, Sustainability 15 (12) (2023) 9434. doi:10.3390/su15129434.

[30] A. Bouaouda, Y. Sayouti, Hybrid meta-heuristic algorithms for optimal sizing of hybrid renewable energy system: A review of the state-of-the-art, Archives of Computational Methods in Engineering 29 (6) (2022) 4049–4083. doi:10.1007/s11831-022-09730-x.

[31] C. Gusain, M. M. Tripathi, U. Nangia, Study of meta-heuristic optimization methodologies for design of hybrid renewable energy systems, Thermal Science and Engineering Progress 39 (2023) 101711. doi:10.1016/j.tsep.2023.101711.

[32] I. Saady, B. Majout, M. S. Adouairi, M. Karim, B. Bossoufi, M. M. Almalki, T. A. H. Alghamdi, Soft computing approaches for photovoltaic water pumping systems: A review, Cleaner Engineering and Technology 22 (2024) 100800. doi:10.1016/j.clet.2024.100800.

[33] M. M. Samy, A. F. Güven, Optimal dimensioning of grid-connected pv/wind hybrid renewable energy systems with battery and supercapacitor storage: A statistical validation of metaheuristic algorithm performance, Scientific Reports 15 (1) (2025) 45658. doi:10.1038/s41598-025-28234-9.

[34] D. Shetty, J. N. Sabhahit, G. Kudva, A methodology to optimize pmsm driven solar water pumps using a hybrid mppt approach in partially shaded conditions, Clean Technologies 6 (3) (2024) 1229–1259. doi:10.3390/cleantechnol6030060.

[35] I. Saady, M. Karim, B. Bossoufi, S. Motahhir, M. S. Adouairi, B. Majout, M. Lamnadi, M. Masud, J. F. Al-Amri, Optimization for a photovoltaic pumping system using indirect field oriented control of induction motor, Electronics 10 (24) (2021) 3076. doi:10.3390/electronics10243076.

ARTICLE IN PRESS

ARTICLE IN PRESS

[36] M. Farhat, O. Barambones, Advanced control scheme optimization for stand-alone photovoltaic water pumping systems, Computation 12 (2024). doi:10.3390/computation12110224.

[37] R. Ben Ammar, M. Ben Ammar, A. Oualha, Photovoltaic power forecast using empirical models and artificial intelligence approaches for water pumping systems, Renewable Energy 153 (2020) 1016–1028. doi:10.1016/j.renene.2020.02.065.

[38] A. Hilali, N. El Ouanjli, S. Mahfoud, A. S. Al-Sumaiti, M. A. Mossa, Optimization of a solar water pumping system in varying weather conditions by a new hybrid method based on fuzzy logic and incremental conductance, Energies 15 (2022). doi:10.3390/en15228518.

[39] I. Saady, M. Karim, B. Bossoufi, N. El Ouanjli, S. Motahhir, B. Majout, Optimization and control of photovoltaic water pumping system using kalman filter based mppt and multilevel inverter fed dtc-im, Results in Engineering 17 (2023) 100829. doi:10.1016/j.rineng.2022.100829.

[40] C. Rahli, M. Ouada, I. Attoui, A. Bouraiou, A. Dekhane, M. Benghanem, A. R. Mebarek, S. Salah, Optimization of photovoltaic water pumping system using nutcracker optimization algorithm, Iranian Journal of Science and Technology, Transactions of Electrical Engineering 49 (2025) 1379–1400. doi:10.1007/s40998-025-00810-9.

[41] M. M. Elymany, M. A. Enany, H. Metwally, A. A. Shaier, Enhanced operation of pvwps based on advanced soft computing optimization techniques, Scientific Reports 14 (2024) 29429–. doi:10.1038/s41598-024-80894-1.

[42] H. M. Bawayan, M. M. Ahmed, M. A. Enany, M. M. Elymany, A. A. Shaier, Modeling and performance assessment of pvwps considering various partial shading scenarios using multi-objective optimizers, Results in Engineering 28 (2025) 107886. doi:10.1016/j.rineng.2025.107886.

[43] J.-Y. Park, S.-J. Choi, A novel datasheet-based parameter extraction method for a single-diode photovoltaic array model, Solar Energy 122 (2015) 1235–1244. doi:10.1016/j.solener.2015.11.001.

[44] S. Lyden, M. E. Haque, Maximum power point tracking techniques for photovoltaic systems: A comprehensive review and comparative analysis, Renewable and Sustainable Energy Reviews 52 (2015) 1504–1518. doi:10.1016/j.rser.2015.07.172.

[45] A. R. Jensen, K. S. Anderson, W. F. Holmgren, M. A. Mikofski, C. W. Hansen, L. J. Boeman, R. Loonen, pvlib iotools—open-source python functions for seamless access to solar irradiance data, Solar Energy 266 (2023) 112092. doi:10.1016/j.solener.2023.112092.

[46] M. Kumar, P. Arora, N. Srivastava, J. Padma, R. Singh, A. C. Bhosale, Optimal sizing of solar photovoltaic water pumping systems by synergizing irrigation patterns and static heads: A comprehensive study in the indian context, Sustainable Energy Technologies and Assessments 77 (2025) 104341. doi:https://doi.org/10.1016/j.seta.2025.104341.

[47] U. Pfeifroth, S. Kothe, J. Drücke, J. Trentmann, M. Schröder, N. Selbach, R. Hollmann, Surface radiation data set - heliosat (sarah) - edition 3 (2023). doi:10.5676/EUM_SAF_CM/SARAH/V003. URL https://wui.cmsaf.eu/safira/action/viewDoiDetails?acronym=SARAH_V003